12-1997

A Dispersive Scattering Center, Parametric Model for 1-D ATR

Dane F. Fuller

AFIT/GE/ENG/97D-05

A DISPERSIVE SCATTERING CENTER, PARAMETRIC MODEL FOR 1-D ATR

THESIS

Dane F. Fuller, First Lieutenant, USAF

AFIT/GE/ENG/97D-05

Approved for public release; distribution unlimited

The views expressed in this thesis are those of the author and do not reflect the official policy or position of the Department of Defense or the U. S. Government

AFIT/GE/ENG/97D-05

A DISPERSIVE SCATTERING CENTER, PARAMETRIC MODEL FOR 1-D ATR

THESIS

Presented to the Faculty of the Graduate School of Engineering

of the Air Force Institute of Technology

Air University

In Partial Fulfillment of the

Requirements for the Degree of

Master of Science in Electrical Engineering

Dane F. Fuller, B.S.E.E.

First Lieutenant, USAF

December, 1997

AFIT/GE/ENG/97D-05

A DISPERSIVE SCATTERING CENTER, PARAMETRIC MODEL FOR 1-D ATR

Dane F. Fuller, B.S.E.E.
First Lieutenant, USAF

Approved:

[redacted]

Andrew J. Terzuoli, PhD, Committee Chairman — 3Dec97 Date
Associate Prof., Dept. of Electrical and Computer Engineering

[redacted]

William M. Brown, Dr Eng, Committee Member — 3 Dec 97 Date
Department Head, Electrical and Computer Engineering

[redacted]

Peter J. Collins, PhD, Committee Member — 3 DEC 97 Date
Assistant Prof., Dept. of Electrical and Computer Engineering

ACKNOWLEDGMENTS

Foremost, I would like to thank all of the members of my thesis committee -- Dr. Andrew Terzuoli, my advisor, for his support and guidance throughout my thesis research and publication, Dr. Rob Williams, my sponsor, for providing me with access to many Wright Laboratory resources, Dr. Steve Rogers for his positive encouragement and professional knowledge in Pattern Recognition, Dr. Bill Brown for his contribution in verifing the viability of the HRR approach to target recognition, Dr. Peter Collins for his assistance in the field of Electromagnetics Scattering and specific input on this document, and Dr. Mike Temple for his active and willing participation late in my research.

Second, I would like to thank Dr. Lee Potter of The Ohio State University for twice hosting me for direct assistance in understanding both his and his students' research.

Lastly, I would like to thank [redacted], my wife, for her love and support including document editing. Her dedication to her own graduate work was an inspiration for me throughout my own studies.

VITA

1Lt Dane F. Fuller was born in [redacted] USA on [redacted]. He recieved his B.S. degree in Electrical Engineering at The University of Texas at Austin in 1993. Subsequently, he was commissioned into the United States Air Force and served in the Phillip's Laboratory Microelectronics Division. He is currently pursuing a M.S. degree at the Air Force Institute of Technology in Electrical Engineeting.

A member of Tau Beta Pi and Eta Kappa Nu, his research interests are in electromagnetic scattering, radar imaging, and pattern recognition.

ABSTRACT

The dispersive scattering center (DSC) model characterizes high-frequency backscatter from radar targets as a finite sum of localized scattering geometries distributed in range. These geometries, along with their locations, can be conveniently used as features in a 1-D automatic target recognition (ATR) algorithm. The DSC model's type and range parameters correspond to geometry and range features according to the Geometric Theory of Diffraction (GTD). Since these parameters are estimated in the phase history domain of the radar signal, the range parameter does provide superresolution in the time domain.

Because the type parameter denotes the frequency response of each localized scatterer based on GTD, there are two considerations when using the DSC model. First, the estimation accuracy of the type parameter is proportional to the relative bandwidth of the radar measurement. Second, non-localized scattering from microwave cavities is approximated by a cluster of scattering centers. However, for most cases, the DSC model still provides stable and discriminatory features for use in ATR.

To demonstrate the viability of feature extraction based on the DSC model's range and type parameters, a typical ATR experiment was performed. The experimental data contains 1204 direct range measurements of four model aircraft of similar size and shape at 0 degrees elevation and from 0 to 30 degrees azimuth. After implementing DSC model feature extraction on this data, a fully-connected, two-layer neural net obtained over 98% classification accuracy. In addition, DSC model feature extraction gives an approximate 85% reduction in the number of features compared to the numerous Fourier bin magnitudes used in template matching approaches to ATR.

TABLE OF CONTENTS

LIST OF FIGURES

LIST OF TABLES

CHAPTER 1
Problem Statement and Overview

Automatic Target Recognition (ATR), the ability for a machine to classify an object it has detected, is an area of continual interest. The classification of targets requires extraction of discriminatory information, and this process is called feature extraction. The extractable features are inextricably tied to the type of sensor used, and I have limited my ATR research to the realm of 1-D, High Range Resolution Radar (HRR).

Several approaches have been proposed for feature extraction in HRR . The most straightforward approach lies in using the magnitude of range bins in range profiles as features. This approach generally denotes template matching [1]; however, template matching is not an optimal approach to ATR because it includes many noisy range bins as features. A different ATR approach is based on finding sinusoids in noise by a sum-of-damped exponentials (DE) model. These superresolution techniques include Prony [2-5], Matrix Pencil [6], and many others. The features of the DE-based scattering models, range and amplitude, have been used for ATR feature extraction, but the DE model simplistically assumes that all scatterering centers on the target have the frequency response of an ideal point scatterer. One high potential improvement to the DE model lies in estimating the frequency response of each scatterering center separately. The improved model is based on the Geometric Theory of Diffraction (GTD) and includes electromagnetic scattering theory as a basis for scattering center modeling. Research in adapting DE models to include GTD has been performed [7, 8], but has had limited implementation into ATR problems. The GTD-based dispersive scattering center (DSC) model presented here is based directly upon Dr. Potter's work at The Ohio State University [8] and this work provides analysis and a proof-of-concept for implementing the DSC model in ATR.

One common limitation of all 1-D approaches is the aspect dependency of the radar measurement of a target. Therefore, one attempts to characterize the target over a specific

aspect range only. However, this fact has not stifled research in 1-D ATR because one may characterize the 360 degree aspect sweep of an entire target piece-wise.

This work focuses upon feature extraction of dispersive scattering centers based on the Geometric Theory of Diffraction (GTD) to perform ATR on radar targets. Chapter 2 contains the background for this paper. Specifically, the chapter describes how the Air Force has performed template matching ATR and presents my literature review and plan of attack.

Chapter 3 first derives the dispersive scattering center (DSC) parametric model from GTD. Then, I compare the accuracy of the DSC model to the aforementioned, non-dispersive, damped exponential model. Additionally, I outline how the DSC model parameters, complex magnitude, type, and range are estimated and discuss the strengths and limitations of the DSC model for use in ATR applications.

Chapter 4 presents the experimental set-up and results of my initial investigative research. By verifying Chiang's published results on a flat disk and a flat plate, these initial experiments are good starting points for illustrating the power and limitations of the dispersive scattering center model for ATR. Additionally, the impact of percent relative bandwidth on DSC modeling is specifically addressed.

Chapter 5 contains two example ATR experiments showing how the DSC model can be implemented to perform ATR. The data for both experiments comes from direct measurements of four model military aircraft. A simple, fully-connected, two-layer neural net is used to classify the targets and results are compiled. Classification accuracy is 99% for the limited experiment and over 98% for the expanded experiment.

Finally, Chapter 6 outlines eight topics for further research. Furthermore, the Appendices supply the reader additional reference information on the topics of Radar Imaging and Pattern Recognition. In addition, Appendix C contains a case study of the Moving and Stationary Target Recognition (MSTAR) ground vehicle data set. This study concludes that the MSTAR data set is unable to provide reliable phase history domain data for DSC estimation.

CHAPTER 2
Background and Plan of Attack

This research project was directed by a merging of interests between myself and my Air Force sponsor, Dr. Rob Williams of the Wright Laboratories Model Based Vision Lab. Thus, my interests in Electromagnetics and Pattern Recognition and my sponsor's work in 1-D radar automatic target recognition (ATR) were successfully integrated in this thesis effort. This chapter outlines the Air Force's current template-based ATR effort, its limitations, and my search for an alternate, phenomenological approach to that same 1-D ATR problem.

2.1 Template Matching ATR

Wright Laboratory's current ATR approach chiefly involves template matching. In template matching, a database of measured or synthetic images, called range profiles, form the templates. An example range profile is given in Figure 2.1. This database contains a template of each target's expected range profile for every viewing angle of the radar. For instance, an index of 17 degrees elevation and 154 degrees azimuth would designate a range profile template which represents the image of the target from this viewing angle. After the template database is compiled, the system is ready to observe and classify targets. When a target is observed, it's viewing angle is estimated and the appropriate templates are compared to the observation. The template with the best match (i.e. highest correlation) is assumed to correspond to the target in the observation, and the observed target is declared to be of the class to which the template belongs. Furthermore, the quality of the template match can be used to derive a confidence level in the classification of the target. Therefore, the features used for classification in template matching are the magnitude of the range profile in each frequency bin; the distance metric for comparing templates to observations is usually Euclidean. Radar Imaging concepts are explained in more detail in Appendix A.

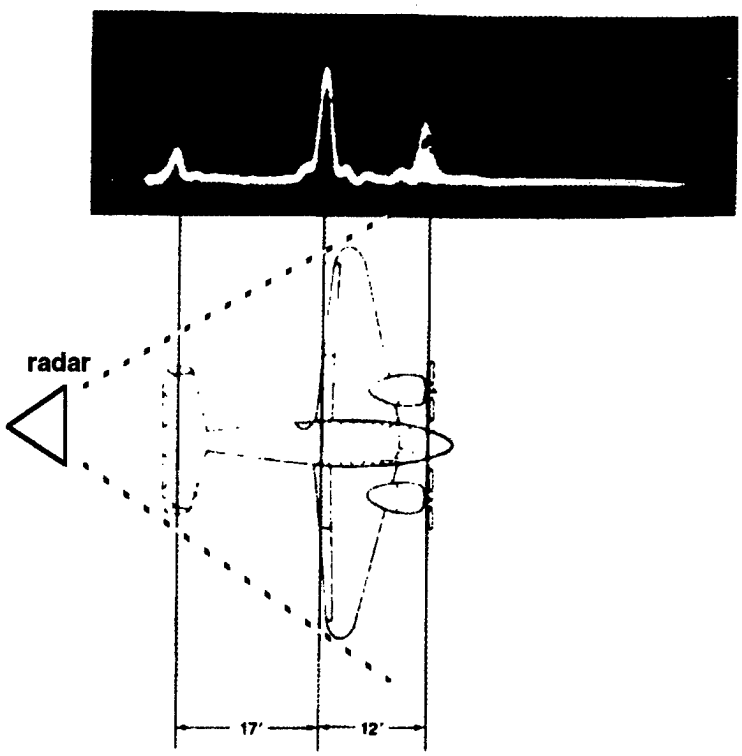

Figure 2.1: Example range profile of an aircraft [12]

After extensive research, Wright Laboratories has recognized many limitations to template matching ATR:

- Increasing the number of classes will linearly increase database size and exponentially increase processing time.
- Range profiles (magnitude only) lack the phase information of the original radar signal; the discarded phase contains valuable discriminatory information.
- A range profile contains a large number of features (one for each frequency bin) and some of these features may be non-discriminatory, actually degrading ATR performance.
- Alignment and normalization of images is a significant complication in template matching.

The solution to these problems lies in finding a smaller, more descriptive, shift invariant set of features and including phase information while extracting them. Therefore, research to develop new approaches to 1-D ATR is ongoing, specifically in feature extraction.

2.2 Plan of Attack

The key to extracting good features from a target's radar signal is to understand the electromagnetic scattering phenomena which create the signal. Upon accepting the task to find a phenomenological approach to 1-D ATR, I began a literature review of the most recent IEEE transactions. I also attempted to build my knowledge in radar imaging through independent study, particularly in the topic of Synthetic Aperture Radar (SAR). In addition, periodic meetings with my thesis committee provided many leads on this topic.

During the process of my background literature review, I discovered an interesting scattering center extraction technique presented at a DARPA Image Understanding workshop. Dr. Lee Potter of The Ohio State University (OSU) described a parametric model, based upon the geometric theory of diffraction (GTD), which he used to analyze the scattering mechanisms in both 1-D and 2-D radar images. Consequently, I obtained a copy of OSU's latest publication in this area [8] and began to focus my literature review and preliminary study towards their approach. I have since then visited OSU, Wright Laboratories, Veda, and Mission Research Corporation to muster resources and coordinate my research with the local community. In addition, I obtained a copy of OSU's 1-D MATLAB code and a copy of the corresponding dissertation by Da-Ming Chiang [9].

I then proceeded to duplicate Chiang's experimental results as a baseline for my own research. Details of these initial experiments are contained in Chapter 4. These investigative experiments helped define guidelines for applying OSU's model to ATR. Based on OSU's work, the feature set I propose for ATR is based on the dispersive scattering center (DSC) model which I derive in the next chapter.

CHAPTER 3
Theoretical Development

Radar returns from large targets at high frequencies can be modeled as a sum of independent scattering centers [10]. These scattering centers are often assumed to be non-dispersive in frequency which simplifies the model and parameter estimation process. However, most scattering centers are dispersive and can elude the simplistic model's ability to characterize the target, especially at high-percent relative bandwidth [8]. The Geometric Theory of Diffraction (GTD) predicts the dispersive nature of scattering mechanisms because certain scattering geometries produce a specific frequency response [10]. Consequently, not only can we model complex targets as a sum of scatterers, but we can also model targets as a sum of scattering geometries. Furthermore, by deducing the scattering geometries on the target, we can extract actual geometrical information about the target which can be used for ATR. This chapter develops the theory behind the GTD-based dispersive scattering center (DSC) model, exploring its strengths and limitations.

3.1 The Dispersive Scattering Center Model

Let the incident field propagating in the +z direction be an infinite plane wave where the field at location z can be described by

$$\vec{\mathbf{E}}^{i}(z) = \vec{\mathbf{E}}_0 e^{-j\frac{2\pi f}{c}z} \tag{3.1}$$

independent of time ($e^{j\omega t}$ is suppressed) where $k = 2\pi f/c$ is the wave number in free space.

GTD as developed by Keller [10] predicts that at high frequencies, the backscattered field related to the incident field and appears to originate from a discrete set of independent scattering centers. The field is given by

$$\vec{\mathbf{E}}^{s}(f,z) \approx \frac{\vec{\mathbf{E}}_0}{|z|} e^{j\frac{2\pi f}{c}z} \sum_{m=1}^{M} \phi_{m,f} e^{-j\frac{4\pi f}{c}\hat{z}\cdot\vec{\mathbf{r}}_m} \tag{3.2}$$

where $|z|$ is the spreading factor of the backscattered field, e^{jkz} is the phase of the incident field at the phase reference, $\phi_{m,f}$ is the frequency dependent magnitude of the scatterer, and r_m is the distance to the m*th* scattering center from the zero phase reference. Furthermore, the two-path phase of each scatterer is given by

$$e^{-j\frac{4\pi f}{c}\hat{z}\cdot\vec{\mathbf{r}}_m} \tag{3.3}$$

as depicted in Figure 3.1.

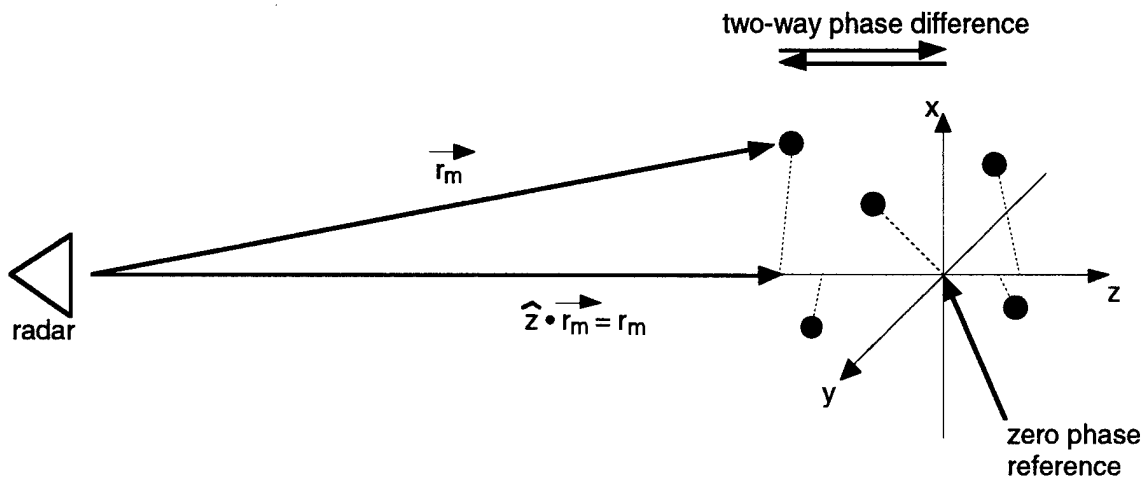

Figure 3.1: Diagram of the scattering centers in the far field

Assuming a given polarization and a normalized field one can rewrite Equation 3.2 as

$$\mathrm{E}(f) = \sum_{m=1}^{M} \phi_{m,f} e^{-j\frac{4\pi f}{c}\hat{z}\cdot\vec{\mathbf{r}}_m} \tag{3.4}$$

GTD predicts that the backscattered E-field magnitude will follow a $(jf)^{\alpha}$ frequency dependence. Therefore $\phi_{m,f}$ can be written

$$\phi_{m,f} = A_m \left(j\frac{f}{f_c} \right)^{\alpha_m} \tag{3.4}$$

and the GTD-based dispersive scattering center (DSC) model down the z-axis of Figure 3.1 is given by [9]

$$\mathrm{E}(f) = \sum_{m=1}^{M} A_m \left(j\frac{f}{f_c} \right)^{\alpha_m} e^{-j\frac{4\pi f}{c} r_m} \tag{3.5}$$

Although one estimates the complex magnitude, A_m, the parameters of interest for ATR are the type parameter, α_m, and the range parameter, r_m. The range parameter gives the location of the scatterer, and the type parameter describes the frequency response of the scatterer. The type parameter is an integer multiple of 1/2 as given by GTD, and a listing of type parameters and their associated scattering geometries is provided in Table 3.1.

Table 3.1: Type parameters and their associated scattering geometries [8]

Value of α	Example Scattering Geometries for a Given α
1	flat plate specular; dihedral
1/2	singularly curved surface
0	pt. scatter; doubly curved surface; straight edge specular
-1/2	edge diffraction
-1	corner diffraction
less than -1	multi-bounce; unresolved or combined mechanisms

The advantage of the GTD-based DSC model is that certain types of scattering (i.e. dihedral, curved edge, straight edge, point scatterer, etc.) will display a continuous change in magnitude with change in frequency. Therefore, as I have stated before, one can essentially model a target as a sum of independent scattering geometries. From Equation 3.5, the magnitude of scatterer m_0 is proportional to $(jf/f_c)^{\alpha}$ where f_c is the center frequency of the "chirped" radar pulse. Therefore, the frequency response of each scatterer determines what the scattering geometry is.

Recall that GTD is a high frequency description of radar scattering phenomena based on the physics of wave propagation. Therefore, the size of a target for which the DSC model can accurately deduce these geometries should be at least several wavelengths long. Also note from Table 3.1 that combined returns will multiply (type parameters are added) producing frequency responses whose type parameters, α, are less than -1.

One important aspect of the DSC model is that it assumes localized scattering centers and does not include the ability to accurately model microwave cavity responses such as those from engine intakes, cockpits, and open hatches. The difficulty with characterizing cavity returns is that there are resonant modes which "turn-on" at different frequencies. Consequently, it is possible for the magnitude of a cavity return to be non-linear, particularly over a large bandwidth. Therefore, these cavities will be estimated as a series of localized scatterers. However, as I shall demonstrate later, this will not prevent the DSC model from discriminating between targets.

3.2 Parameter Estimation

The straight-forward approach for estimating the DSC parameters requires a global search for A_m and r_m individually for each possible type parameter, α_m. This search must be performed for all M scattering centers simultaneously. Obviously this straight-forward approach creates a significant computational challenge. Fortunately, in the dissertation, "Parametric signal processing techniques for model mismatch and mixed parameter estimation," Chiang's primary effort was in finding a computationally efficient way to estimate these parameters [9]. Chiang proposed two main simplifications:

- while estimating A_m and r_m, treat the type parameter, α_m, as continuous estimating it simultaneously and
- replace the search for a global minimum with a search for a local minimum by first computing good initialization points for α_m, A_m, and r_m.

To accomplish the latter, Chiang proposed a surrogate scattering center model based on the heavily published, damped exponential (DE) model estimation [2-6].

In this manner – even though the DSC model is more accurate -- one can gain significant computational efficiency by first using the DE model. After estimating the DE model parameters, the DSC model parameter initialization points can be derived from these DE parameters. Using these initial points, a Newton-Raphson iterative optimization procedure can refine the DSC model parameter estimations. The generic damped exponential model is [11]

$$x(f_n) = \sum_{m=1}^{M} D_m p_m^n \tag{3.6}$$

When used to describe electronic scattering for a single polarization, the DE model can be compared to the DSC model by implementing variable substitution as performed by Chiang [9] where

$$E(f) = \sum_{m=1}^{M} A'_m \beta_m^{\frac{2\pi f}{c}} e^{-j\frac{4\pi f}{c} r_m} \tag{3.7}$$

Notice that the DE model in Equation 3.7 differs from the DSC model in Equation 3.5 by the second factor where $\beta_m^{2\pi f/c}$ replaces $(jf/f_c)^{\alpha}$. These two factors define how the frequency dependence of the magnitude of each scatterer is represented differently in each model. Although they are different, the two models correspond for the case of $\alpha=0$ and $\beta=1$. This condition represents a target composed of ideal point scatterers which are non-dispersive in frequency. For all other types of scatterers, the DE model will not correctly represent the frequency dependence of the scattering center magnitudes [9].

Additionally, the DE model will correctly estimate the range parameter for the case of a single scatterer at high frequency. However, for the case of multiple, non-ideal point scatterers, the simple DE model incurs a bias in the range estimates [9]. In the DSC estimation algorithm, this bias is corrected by an iterative optimization procedure.

I conclude this section with a summary of the type parameter estimation process as developed by Chiang [9]. First the DE model parameters are estimated using the Matrix Pencil method [6]. Then, the alpha initialization point is obtained from an affine transformation of the DE pole modulus. This transformation is derived in Chiang by comparing the binomial and Taylor series expansions of the DE and GTD models. After obtaining the initial point, α_m is estimated as a continuous value along with A_m and r_m. Finally, the estimated, continuous value of α_m is mapped back to the discrete values of integer multiples of 1/2. This final mapping is according to the weighted distance derived from the Hessian Matrix.

3.3 Limitations of the DSC model

Although the DSC model is more accurate than the DE model, and its parameters more geometrically descriptive than a range profile, the DSC model has several limitations. The

relative bandwidth of the radar return as well as the number of frequency samples can effect accuracy of DSC model parameter estimation. Furthermore, the model order, M in Equation 3.5, must be preselected by the system designer to provide a good representation of the target. These issues are largely application-specific and must be considered when applying the dispersive scattering center model to any particular problem. The primary design issues of signal to noise ratio (SNR), percent relative bandwidth, and model order are discussed below.

3.3.1 Signal to Noise Ratio

As with all parametric models, low SNR can degrade parameter estimation. Specifically, the DSC model can be sensitive to noise because it effects type parameter estimation in particular. However, through coherent averaging over several measurements of the target, SNR can be greatly increased [12]. Although SNR is a concern in template matching, there is inherent averaging in the template formation process [1]. Because SNR is an important but not unique limitation to the DSC model, the reader is referred to Chiang's Cramer-Rao Bound analysis for specific examples of how SNR impacts DSC model accuracy [9].

3.3.2 Percent Relative Bandwidth

The concept of percent-relative bandwidth is important in DSC modeling. While a large relative bandwidth emphasizes the dispersive nature of scattering centers and biases the DE model's range estimates, too small of a bandwidth will degrade alpha parameter estimation in the DSC model. Figure 3.2 illustrates the advantage of having a large percent-bandwidth for alpha estimation.

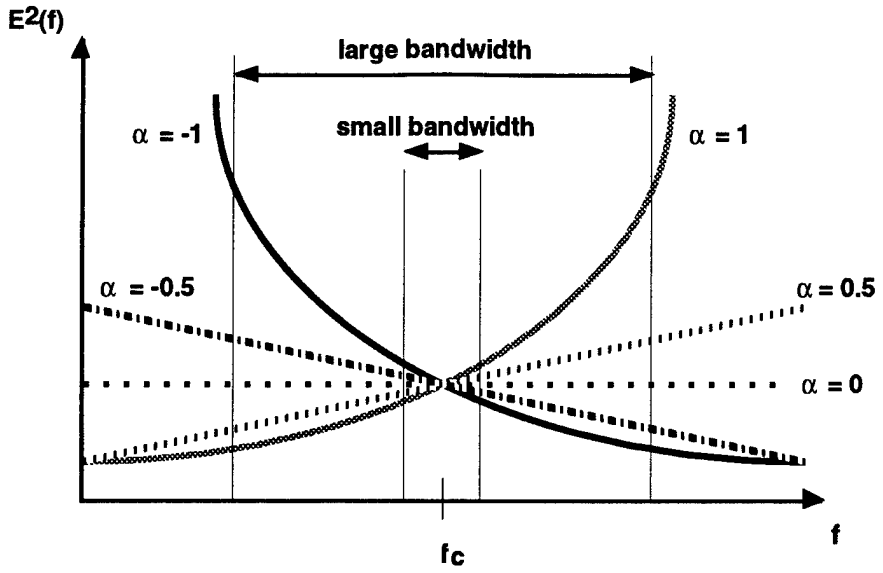

Figure 3.2: Illustration of the advantage of large percent bandwidth

In Figure 3.2, the curves represent different type parameters and are better distinguished over a large-percent relative bandwidth. Furthermore, the DSC process of converting the discrete alpha to a continuous parameter, estimating it, and then mapping it back to a discrete value complicates its estimation accuracy over a small-percent relative bandwidth.

3.3.3 Model Order

The number of scatterers estimated defines the model order of the DSC model, is chosen by the user, and is highly dependent upon the application. Some factors include

- complexity of the target being modeled,
- conditions of signal generation (bandwidth, SNR, etc.),
- types of scattering mechanisms one wants to detect,
- the range resolution desired,
- the modeling accuracy required, and
- the type of algorithm that will be using the model parameters as inputs.

In general, there are predictable consequences for both underfitting and overfitting the model and understanding these consequences is helpful in making the decision of what model order to prescribe.

If the model is underfit (M too small), the estimator will tend to combine the description of neighboring scatterers into one. When this combination occurs, neither of the neighboring scatterers are correctly characterized. For a combination of two scatterers, the model will estimate a range that is between the two scatterers and an alpha that is typically an addition of the two scatterers' type parameters. If the model is overfit (M too large), the estimator will tend to model spurious scatterers which are located in the low energy areas (low amplitude peaks) of the image. The type parameters for such returns are usually very low (i.e. $\alpha = -3$ or less).

For an ATR application, the model order should be chosen solely to obtain the best classification results. If classification error is plotted with respect to model order the correct model order will be where there is a *knee* in the curve as shown in Figure 3.3.

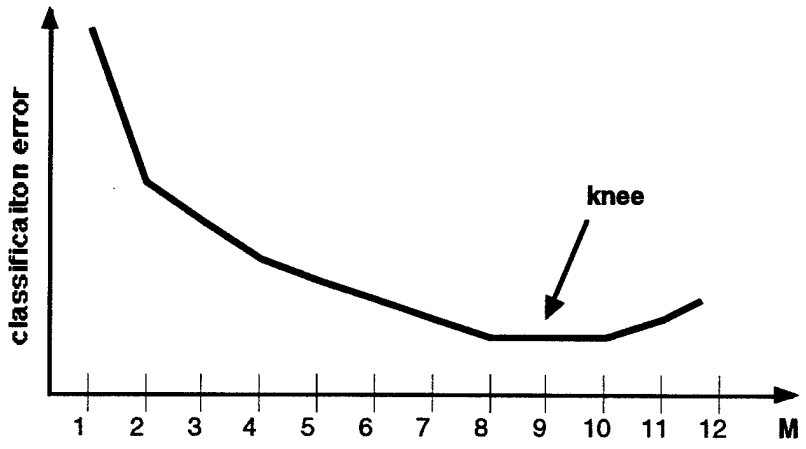

Figure 3.3: The *knee* in the curve where M provides the best classification.

This type of model order optimization is performed in Section 5.2.2 where the best classification accuracy averaged over 1000 runs is used to determine M. Also in that section is an example of 98% classification accuracy even with an underfit model. Therefore, I assert that optimal DSC modeling does not perfectly relate to optimal classification accuracy and

parameters with seemingly large variance may still be able to discriminate between given classes. This assertion will be supported in the results of Chapter 5.

CHAPTER 4
Initial Experiments

My initial experiments were investigative, attempting to verify Dr. Potter's published results as a foundation for my own independent thesis research. In the article "A GTD-Based Parametric Model for Radar Scattering," Dr. Potter chose two simple targets to demonstrate his technique [8]. The first target is a computer-simulated, 0.25 m radius, perfectly electrically conducting (PEC) disk. The second is a compact range measured, 4 ft square, PEC plate. To duplicate Potter's results, I measured both a disk and plate of similar size and orientation over similar frequencies and polarization. Dr. Potter's test data and my test data are given in Tables 4.1 and 4.2.

Table 4.1: Dr. Potter's test data

Target	Pol.	Frequency (GHz)	Elevation	Azimuth
0.5 m diam. PEC disk	HH	1 : 0.01 : 3	0 degrees	15 degrees
4 ft square PEC plate	HH	2 : 0.02 : 18	44 degrees	5.3 degrees

Table 4.2: Test matrix for initial experiments

Target	Pol.	Frequency (GHz)	Elevation	Azimuth
1 ft diam. PEC disk	HH	6.2 : 0.01 : 18.2	0 degrees	15 degrees
1 ft square PEC plate	V V	6.2 : 0.01 : 18.2	~ -5 degrees	44 degrees

For these two experiments, all measured data was taken at the AFIT radar measurement range and I implemented a1-D code developed in Dr. Chiang's dissertation research [9] to estimate the parameters of the scattering centers of both targets. As stated in Section 3.2, there are two conditions which must be met to insure accurate type parameter estimation: a high signal to noise ratio and a large percent-relative bandwidth. I met the first criteria by taking my

measurements in an anechoic chamber, implementing coherent integration over 64 returns, and using background subtraction to provide an extremely high SNR. I met the second criteria by taking a large frequency sweep (6.2 to 18.2 GHz) providing 98% relative bandwidth. Meeting the second criteria was particularly important since both the disk and plate were only a few wavelengths in extent. My results and how well they correspond to Dr. Potter's published results are discussed individually for each target in the following sections.

4.1 Circular Disk Measurement

The circular disk is considered a simple canonical target. For this, I actually measured the frequency response of my disk while Dr. Potter used a computer simulation to compute the frequency response of their disk. The simplicity of this target is demonstrated in the following sections where I examine the compact range measurement and its estimated scattering center parameters, and compare them to Dr. Potter's results. A diagram of the circular disk measurement is given in Figure 4.1.

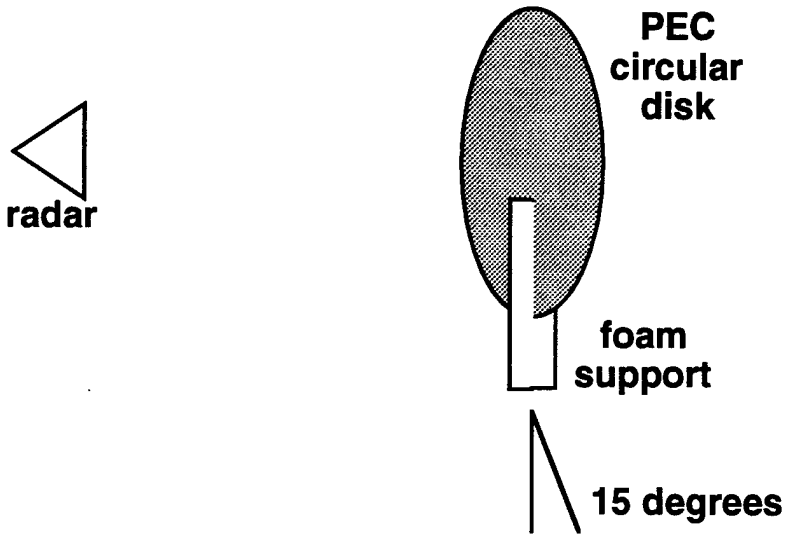

Figure 4.1: PEC circular disk measurement

Figure 4.2b contains the measured radar cross section (RCS) of the disk versus frequency and Figure 4.2a contains the range profile of the disk with DSC parameters shown as vertical lines.

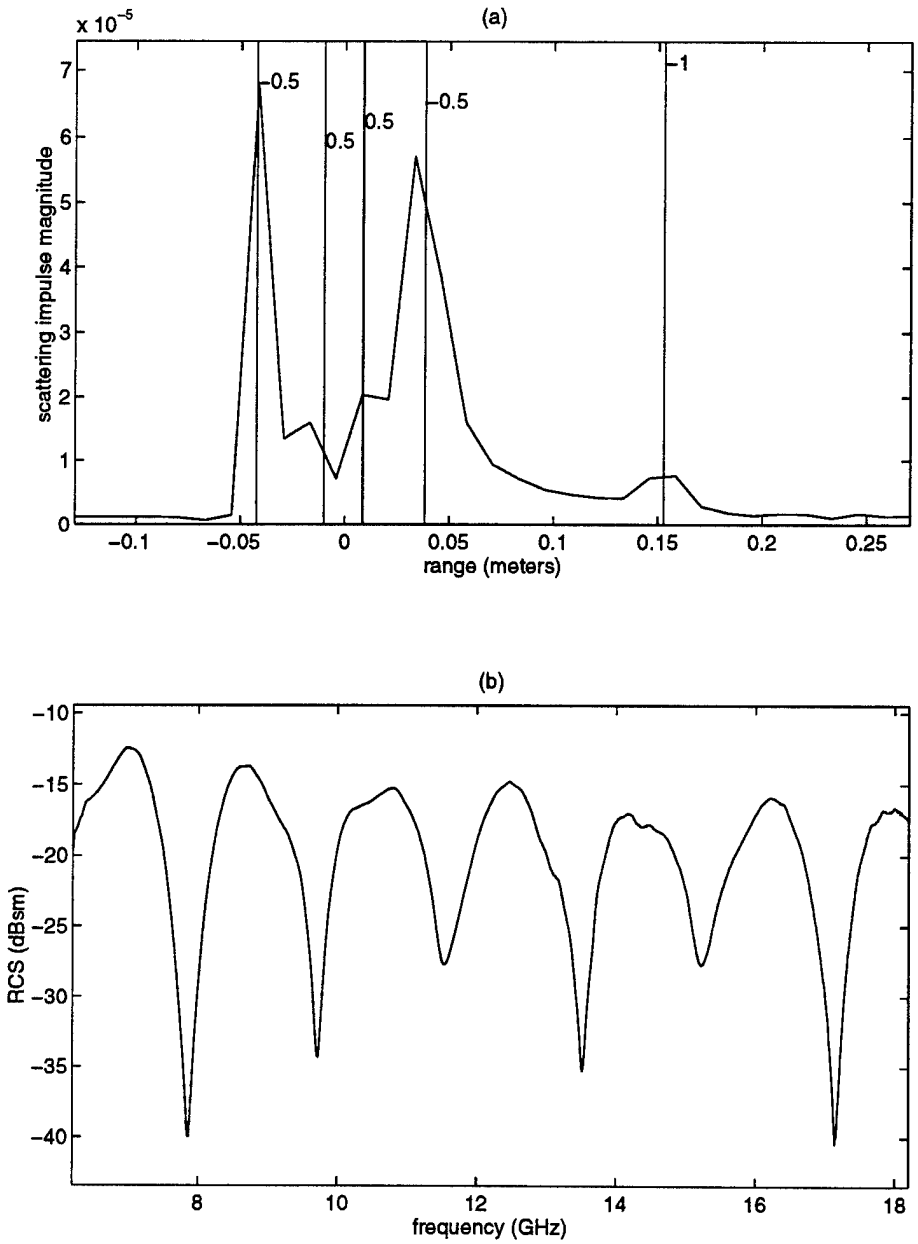

Figure 4.2: Measurement of the circular disk: (a) range profile (b) RCS

Note the periodic nulls in the frequency response of Figure 4.2b. This is characteristic of a two scattering center interference pattern. Thus, the disk will have two primary scatterers and this

fact is precisely why the disk is a simple target. These scattering centers are represented by the two large spikes in the range profile of Figure 4.2a.

4.2 Disk Experiment Comparison

For comparison with my DSC model estimated scatterers, Figure 4.3 contains Dr. Potter's published results. Note that I have estimated five scatterers of interest in the range profile of Figure 4.2a. These correspond well to the GTD estimate given in Figure 4.3. The foam support returns, two peaks designated with $\alpha = 1/2$, are correctly estimated since the foam cylinder creates a singularly curved surface scattering mechanism. Note from Figure 4.3 that,Dr. Potter did not simulate the foam supports.

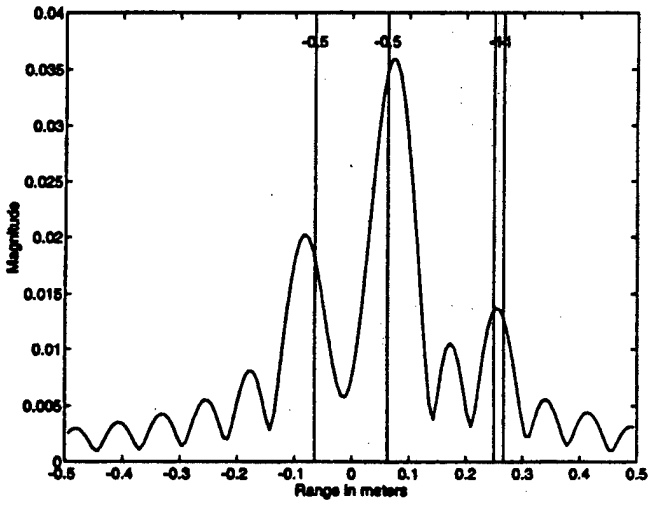

Figure 4.3: Dr. Potter's result for the simulated PEC circular disk [8]

A comparison of the theoretical and estimated scattering center parameters, α_m and r_m, are in Table 4.3. A scaling factor of 1.64042 m/ft is used to relate the measured 1 ft diameter disk to the simulated 0.5 m diameter disk.

Table 4.3: Theoretical and Estimated Scattering Center Parameters of the Disk

Theoretical		Potter simulated		DSC measured			DE est.
range (m)	type	range (m)	type	range (m)	scaled (m)	type	range (m)
-0.0647	-0.5	-0.0650	-0.5	-0.0416	-0.0682	-0.5	-0.0638
0.0647	-0.5	0.0628	-0.5	0.0391	0.0641	-0.5	0.0628
0.2500	-1	0.2659	-1	missing	-	-	missing
0.2475	-1	0.2489	-1	0.1536	0.2519	-1	0.2452
-	-	-	-	-0.0093	-	0.5	-
-	-	-	-	0.0094	-	0.5	-

From Table 4.3, the results of the DSC model estimation are in line with theoretical results. Two corner diffractions, $\alpha = -1$, are estimated. This result illustrates the way in which the DSC model provides superresolution in the time domain. These are not resolved by two peaks in the image (Fourier resolution), but are resolved by the scattering center model. The two scatterers are not resolved in my disk estimation, either because they were so close together or because my measurement had less fidelity than OSU's disk simulation data. At this time I would also like to note why the vertical lines in the images are not perfectly aligned with the peaks. This is due to the fact that the peaks are an artifact of Fourier processing which has less resolution than the DSC model. Therefore, any supposed peak is an interpolation (Figure 4.3) or is simply not resolved (Figure 4.2) in the image domain. This experiment is a prime example of how one can use the DSC model as a measurement analysis tool because of its accuracy and demonstrated superresolution. Use of the DSC model as an analysis tool is discussed in the next section.

4.3 The DSC Model as a Diagnostic Tool

Although the focus of this document is ATR, it is appropriate to highlight some of the diagnostic abilities of DSC modeling at this time. One of the benefits of the DSC model is its predictability. Since large scattering centers on a target can often be predicted by simple inspection, the DSC model enables us to verify the locations and types of scattering we expected to exist. This quick verification can increase one's confidence in a given measurement.

In addition, a poor DSC modeling of the target can be a strong indication of a corrupted measurement.

After verifying the scattering centers one expects to see on the target, further analysis allows the DSC model to highlight target-range interactions such as the foam column returns in Figure 4.1. The ability to detect and isolate these interactions by imaging alone is often impossible, because in the image, the relative magnitudes of such returns are unpredictable. Through range and type parameters, the DSC model may allow a measurement range operator to quickly separate a predicted target return from a pedestal or ground interaction. In addition, constructive and invasive attempts to reduce these interactions will be mirrored in subsequent DSC modeling.

As with target-range interactions, one can use the DSC model to track changes in radar cross section (RCS) which come from the application of radar absorbing material (RAM) or shaping of a target. Often, large sources of scattering can be determined by inspection of the target image alone; however, this process is increasingly difficult for stealthy targets where multi-bounce returns may also be significant. The radar stealth design process could certainly benefit from the DSC model's ability to identify the types of scatterers present on a stealthy target.

4.4 Square Plate Measurement

After completing the circular disk experiment, I felt confident that I was correctly implementing the DSC model estimation algorithm. However, I also wanted to verify OSU's published results for a square plate target, especially since the plate contains different scattering mechanisms than the disk. A diagram of my square plate measurement is shown in Figure 4.4.

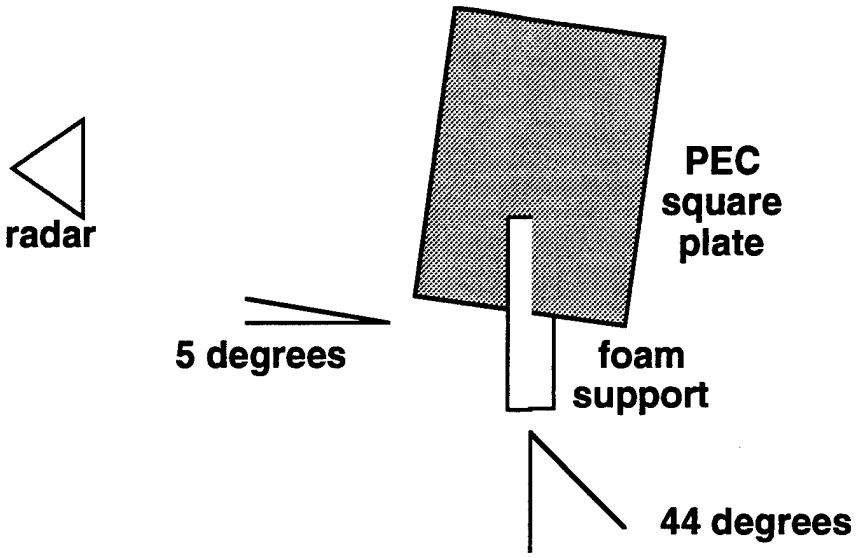

Figure 4.4: Diagram of PEC square plate measurement

Note that in Tables 4.1 and 4.2 I used a different orientation than in the published measurement, so I changed the polarization accordingly. This accommodation resulted in an identical measurement. Figure 4.5a contains the range profile of the plate with DSC parameters shown as vertical lines while Figure 4.5b shows the measured RCS of the field which the DSC model used for parameter estimation.

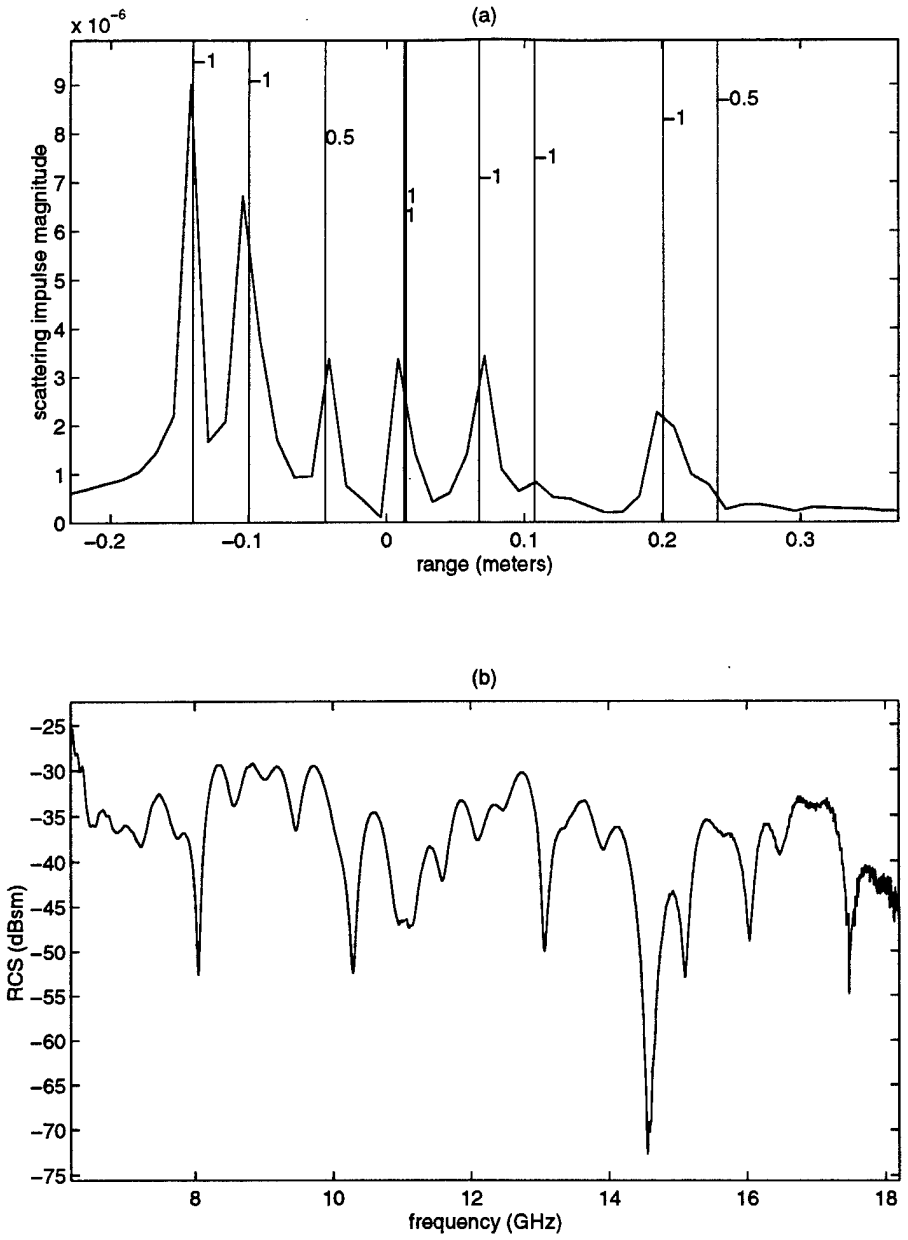

Figure 4.5: Measurement of the square plate: (a) range profile (b) RCS

Note that I have highlighted 9 points of interest in the range profile, all of which were estimated by the DSC model. The primary returns of interest are the corner returns of α = -1 of which there are four: two front corners and two back corners. The back corners are lower in magnitude because of the polarization of the wave, and the last corner is barely resolved in the

range profile; however, the DSC model is able to find it. The third scattering center, $\alpha = 0.5$, is again from the foam column, and the others are all undesignated, or multi-bounce returns.

4.5 Plate Experiment Comparison

For comparison to my results in Figure 4.5, Figure 4.6 contains Dr. Potter's published results which I was attempting to verify.

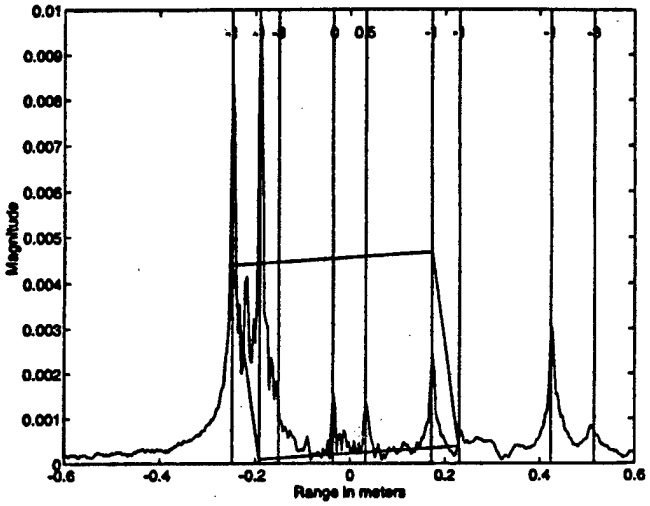

Figure 4.6: Dr. Potter's result for the measured PEC square plate [8]

The location of the corner diffractions is illustrated by the square plate overlay in Figure 4.6. There is a high correspondence between the two estimates, especially in the four corner diffractions. Therefore, I am satisfied that the DSC model is robust enough to provide accurate characterization of simple targets. The next chapter, ATR Proof of Concept, shows how the DSC model can be applied to complex targets such as aircraft.

CHAPTER 5
ATR Proof of Concept

ATR performance is greatly increased when the spatial and geometrical description of a target is deduced. Since the labeling of scattering geometries on a target provides this description, the DSC model has great potential in ATR applications. For instance, the relative magnitudes of scatterers obtained from the range profile have had limited success because of the high variability of scatterer magnitude with small changes in aspect angle and polarization. In contrast, the type parameter is a geometrical descriptor of the target and has less variability with aspect angle or polarization. Therefore, it is my belief that the dispersive scattering center model can provide a suitable and efficient means for target discrimination in ATR. I have conducted two proof-of-concept experiments to demonstrate how the DSC model can distinguish between targets. The first is over a limited aspect range and the second is over an expanded aspect. Both contain four aircraft targets of similar size and shape.

5.1 Limited Experiment

Demonstrating the usefulness of the dispersive scattering center model parameters as features for ATR was the final goal of this work. In order to illustrate how these parameters can effectively be used in ATR, I have conducted a simple four-class ATR experiment. The measurement parameters for all four targets are given in Table 5.1.

Table 5.1: Measurement parameters for the limited ATR experiment

Target (1/48th scale)	Pol.	Frequency (GHz)	El (deg)	Az (deg)
PEC F-15	HH	6.2 : 0.01 : 18.2	0	4 : 0.04 : 6
PEC F-4	HH	6.2 : 0.01 : 18.2	0	4 : 0.04 : 6
PEC F-14 (forward wing)	HH	6.2 : 0.01 : 18.2	0	4 : 0.04 : 6
PEC F-14 (swept wing)	HH	6.2 : 0.01 : 18.2	0	4 : 0.04 : 6

This data collection produced 51 samples of each target between 4 and 6 degrees azimuth. These measurements represent the frequency response of each target over a small 0 by 2 degree window; there is no change in elevation over these measurements. Although a square window with extent in both elevation and azimuth (i.e. 5 degrees by 5 degrees) is usually used to represent targets in ATR applications, this measured data will still provide a limited first look into how the DSC model can successfully be applied to more extensive data sets.

5.1.1 Feature Extraction

For a simple demonstration, I decided on a DSC model order of five. Therefore, there are five pairs of distance and type parameter available to use in the classification algorithm. An example fifth-order scatterer estimation for the F-4 at 5 degrees azimuth is given in Figure 5.1.

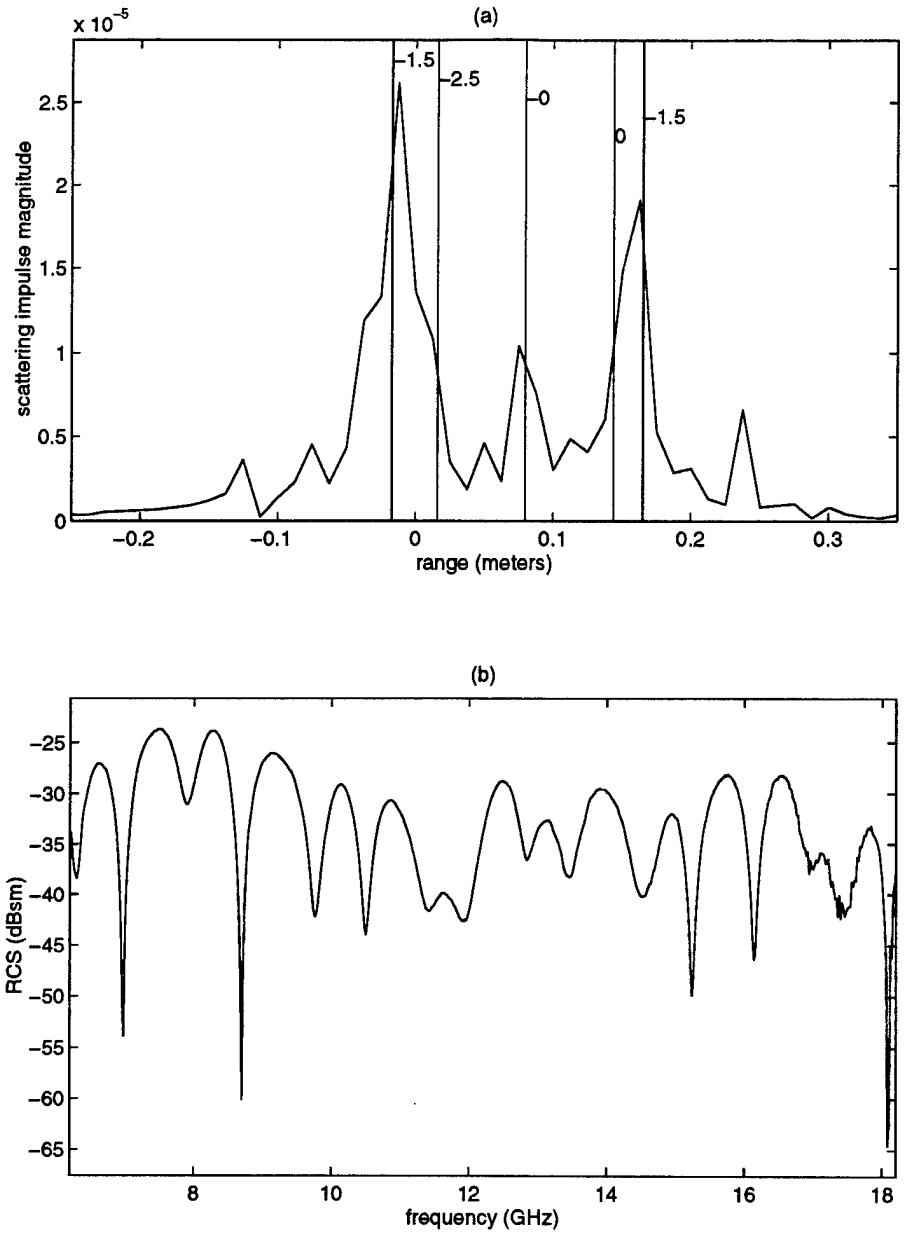

Figure 5.1: Example scatterer estimation of F-4 at 5 degrees azimuth: (a) range profile (b) RCS

It is obvious that a model order of five will not capture all of the scattering centers in as complex a target as an F-4, where dozens of localized scatterers of various geometries could certainly be predicted and perhaps modeled. However, if the largest five scatterers which I estimated do not exactly model the target, they may sufficiently represent the target class for this data set anyway. This principle is very important in ATR. Simply stated, the criteria for

ATR is not that these estimated dispersive scatterers are precisely modeled, but rather, that they are

- reasonably stable across all samples of one class and
- discriminatory between samples of different classes.

Through preliminary DSC model estimations, clustering, and feature analysis I deduced that a fifth order DSC model will sufficiently characterize the targets for this limited data set.

A measurable benefit of clever feature extraction is an increase in algorithm efficiency. For the four targets in this experiment there are 50 range bins on target for an equivalent 2 ft. resolution on a fully-scaled fighter aircraft. Template matching HRR ATR approaches generally expect 1 ft. resolution on target for over 150 range samples to cover targets of all sizes. This means that a template matching algorithm has to manipulate 150 features, the magnitude of the radar return in each bin, in order to perform ATR. Thus, the memory needed to store all of the templates, as well as the processing demand needed to perform the template matching, can be enormous.

In my fifth order DSC approach, I settled on nine features -- a significant savings over the 150 features needed for template matching. The nine features I chose were the type parameters of all five scattering centers, and the distances between the scatterers. These distances were summarized in four shift-invariant features, the distance of each of the four other scatterers from the first scatterer. These four distance features were chosen because, in general, the first scatterer is the most stable scattering center in the radar return. This stability is derived from the absence of intermediate and late-time returns consisting of multi-bounce and shadowed scatterers which are more aspect dependent and unpredictable. Notice, however, that with these four values, a linear combination of two of them can derive the distance between any two scatterers. Due to the simplicity of this linear combination, all distances between scatterers are readily accessed by a neural net if any should prove useful for class discrimination.

5.1.2 Classification Results

To perform ATR, I used a simple, fully-connected, two-layer neural net with four hidden nodes. A diagram of the neural net configuration is shown in Figure 5.2, and general discussion of pattern recognition concepts are presented in Appendix B.

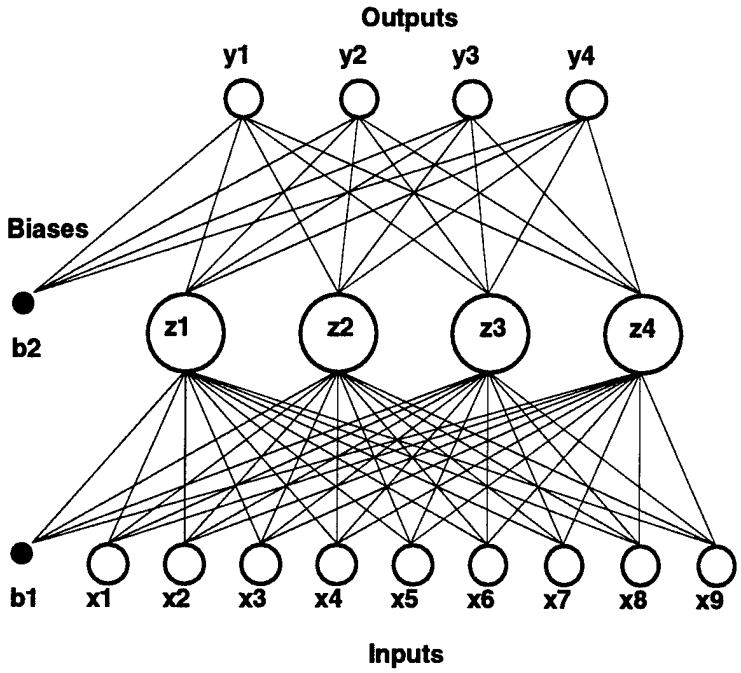

Figure 5.2: Fully-connected, two-layer net with four hidden nodes.

I trained the neural net on the nine features estimated from every odd sample (26 total) of the 51 samples for each target. The remaining 25 even samples were reserved for testing the classification performance of the neural net. I conducted 100 training sessions to a sum squared error of less than 0.02 using the "trainbpx" algorithm from the MATLAB Neural Network Toolbox with the following default parameters:

1. epochs = 1000,
2. learning rate = 0.01,
3. learning rate increase = 1.05,
4. learning rate decrease = 0.7,

5. momentum = 0.9, and

6. error ratio = 1.04.

In addition, I shuffled the training data and randomly initialized the weights on each session. I also normalized my inputs since all weights were using the same learning rate.

Of these 100 training sessions I averaged a test data classification accuracy of 98.25%, and found a maximum accuracy of 99%. The confusion matrix for the typical 99% accurate neural net is presented in Table 5.2.

Table 5.2: Confusion matrix of typical net which obtained 99% test data accuracy

		declared		
actual	F-14b	F-14f	F-15	F-4
F-14b	25	0	0	0
F-14f	0	25	0	0
F-15	0	0	25	0
F-4	0	1	0	24

The one misclassification of Table 5.2 represents an outlier which was never correctly classified in all 100 training runs. Although it is not readily apparent why this one pattern was difficult to correctly classify, it is my belief that an increase in model order, M, would certainly improve average classification accuracy and likely obtain 100% accuracy. However, optimization of the classifier was not the goal of this simple ATR experiment; rather, my goal was to provide a simple proof of concept to assure that the DSC approach can be applied to ATR of complex targets.

Furthermore, two remarkable concepts were illustrated by this experiment. First, the inability of the DSC model to characterize cavity responses from the engine intakes of the aircraft did not ruin its ability to discriminate between targets. Second, this modeling deficiency is in addition to an underfit model which also did not significantly hinder classification.

5.2 Expanded Experiment

Now that I have demonstrated the DSC model's ability to perform ATR, the goal of the expanded experiment is to explore just how robust the approach is on a larger, more extensive set of data. The data for the expanded experiment covers a much larger aspect and uses double the frequency step as that of the limited experiment. Measurement parameters for the expanded experiment are given in Table 5.3. This test matrix produced 301 samples of each target.

Table 5.3: Measurement parameters for the expanded ATR experiment

Target (1/48th scale)	Pol.	Frequency (GHz)	El (deg)	Az (deg)
PEC F-15	HH	6.2 : 0.02 : 18.2	0	0 : 0.1 : 30
PEC F-4	HH	6.2 : 0.02 : 18.2	0	0 : 0.1 : 30
PEC F-14 (forward wing)	HH	6.2 : 0.02 : 18.2	0	0 : 0.1 : 30
PEC F-14 (swept wing)	HH	6.2 : 0.02 : 18.2	0	0 : 0.1 : 30

5.2.1 Accuracy Optimization

In order to determine the best classification performance possible in the expanded experiment, one must find the model order, M, and the number of hidden nodes, N, which will give the best classification accuracy for the test data. Using a similar process as with the limited experiment, I divided the data set between training (odd samples) and testing (even samples) data. Also, the same type and distance features as were used in the limited experiment are extracted for each sample. One deviation from the limited experiment is in frequency sampling. Through analysis of the impact of sampling on DSC performance, I determined that a frequency step of 100 MHz was sufficient for accurate modeling in this case. This down sampling results in an unambiguous range that is over twice the target extent.

As stated in Section 3.3.3, the choice of DSC model order for an ATR application should be based on classification accuracy. Likewise, the choice of the number of hidden nodes in the neural net should be based on accuracy also. Therefore, I chose model orders from 4 to 9 with node counts from 4 to 8 and calculated the test data classification accuracies (mean, median, and maximum) over 1000 training runs for all combinations of model order and node count. The resulting surface plots for mean, median, and maximum accuracies are given in Figure 5.3.

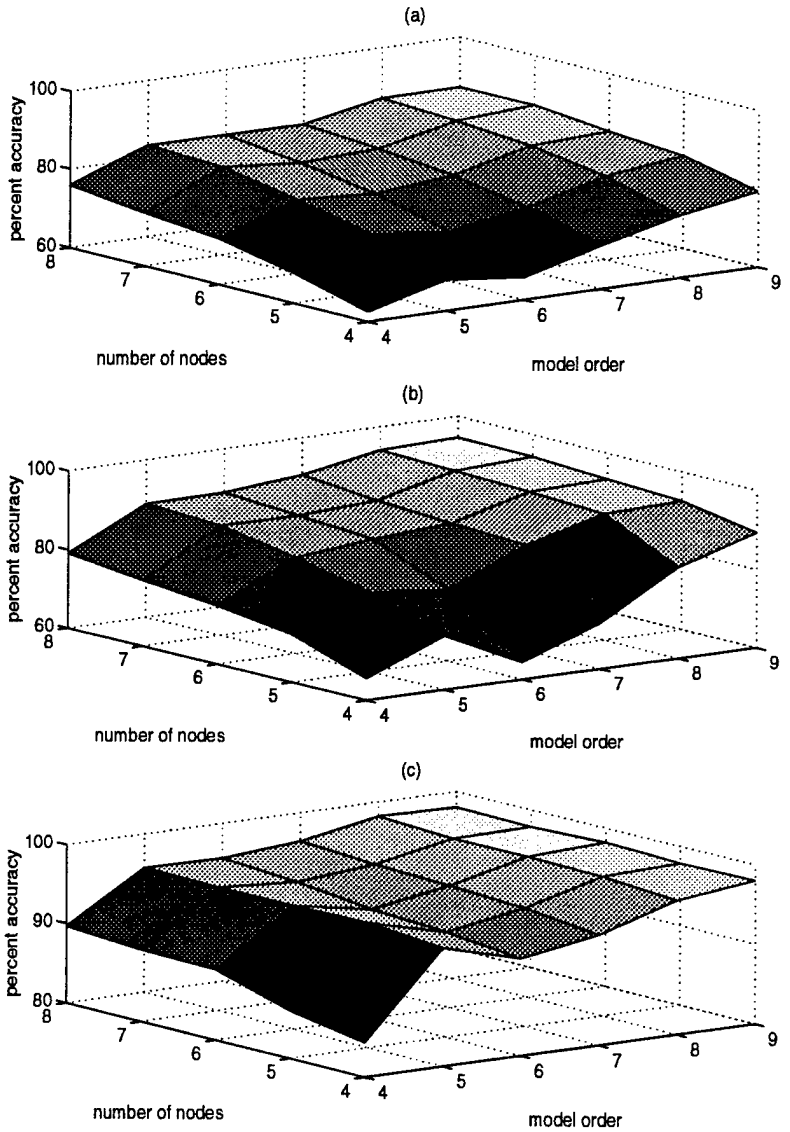

Figure 5.3: Accuracies of the neural net classifier versus model order and node count: (a) mean (b) median (c) maximum

For the case of model order 9 and nodes 8, a histogram of accuracies over the 1000 training runs is presented in Figure 5.4.

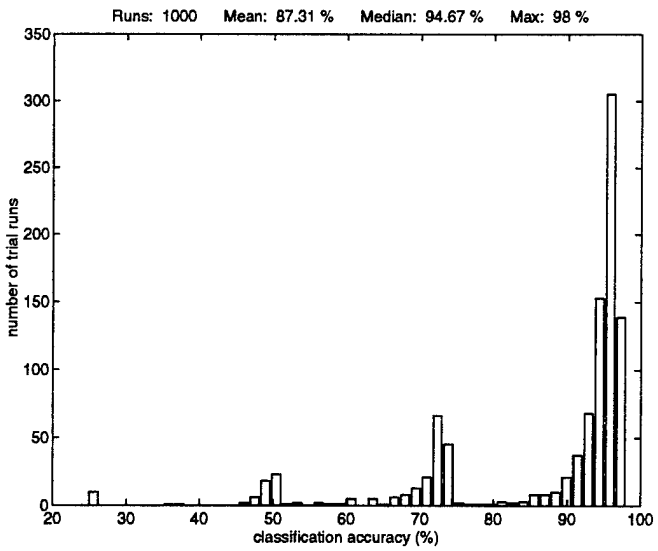

Figure 5.4: Histogram of classification accuracies for model order 9 and nodes 8.

Notice that there are 4 groups of classification accuracies at 25%, 50%, 70%, and 95%. These four groupings represent the cases of three, two, one, and none of the classes being completely unrecognized by the neural net. The reason why this occurs is that each training run has a different initial starting point and faces different local minimums in backpropagation. It would be theoretically possible for all of these trial runs to reach the maximum accuracy with enough training time; however, I limited my training to 1000 epochs on each run. I did not train for an extensive number of epochs because I did not want to over train and memorize the training data. This over training would result in the net's inability to generalize with respect to the test data or other observations. Ultimately, the grouping of training accuracies as shown in Figure 5.4 is the motivation for considering median training accuracies in Figure 5.3.

The best performance of all runs was for 6 nodes and a model order of 9 at 98.17% test accuracy. The confusion matrix for this case is presented in Table 5.4.

Table 5.4: Confusion matrix of best performing net which obtained 98.17% test data accuracy

		declared		
actual	F-14b	F-14f	F-15	F-4
F-14b	150	0	0	0
F-14f	1	149	0	0
F-15	0	0	145	5
F-4	1	3	1	145

5.2.2 Results and Conclusions

The best classification accuracies for the expanded experiment over all is obtained at a model order of 9 and 8 hidden nodes. Since the gradient of classification accuracy at this point is close to zero, I conclude that I have reached a point of diminishing returns. Therefore, I state that approximately 98% classification accuracy may be obtained for this data set. This is an encouraging result considering that I have modeled the four targets over such a large range in aspect.

Since the focus of the DSC model is upon the type parameter, I wanted to understand how important the alpha parameter is to target classification; therefore, I duplicated the expanded experiment without the type parameter, α. The best classification accuracies for 100 runs were 79.22%, 88.67%, and 93.67% for mean, median, and maximum respectively. This represents a significant decrease in accuracy without the type parameter.

For comparison, I analyzed accuracy over the same model orders and number of hidden nodes for a data set containing only the first half of the target measurements (i.e. smaller aspect range). The accuracies for this reduced data set are presented in Figure 5.5.

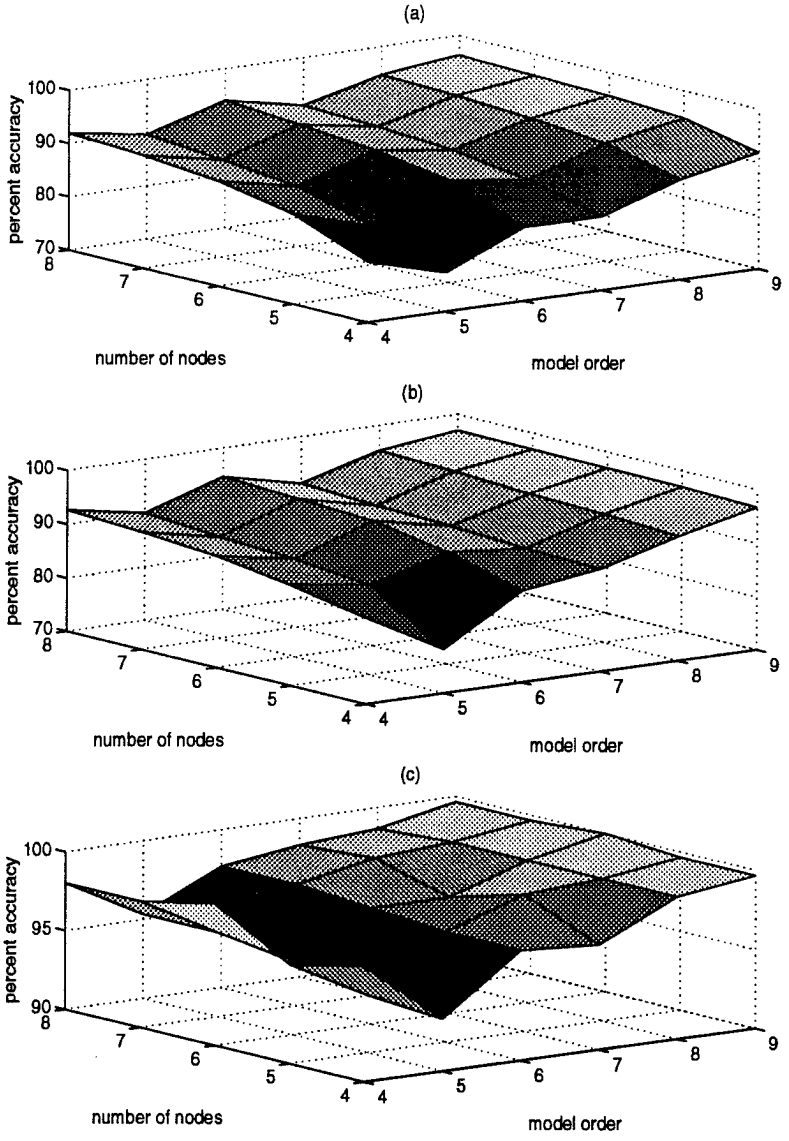

Figure 5.5: Accuracies of the neural net classifier for a 50% reduced aspect: (a) mean (b) median (c) maximum

As expected, the results in Figure 5.5 show slight improvement due to the larger aspect set in Figure 5.3. Specifically, at model order 9 and 6 nodes 100% accuracy is achieved. This additional analysis demonstrates the DSC model's sensitivity to aspect angle and its ability to perform ATR for other aspect ranges. Certainly, as stated in Chapter 1, one neural net cannot separate all targets over 360 degrees in aspect. Therefore several nets will have to be maintained to represent all targets from every aspect.

I conclude Chapter 5 by reiterating the advantages of DSC based ATR versus template matching. Although it is significant that I received a high accuracy in the expanded experiment, it is more important that I also realized a large efficiency of features. The DSC model feature extraction used here provides an approximate 85% reduction in number of features compared to the numerous Fourier bin magnitudes used in template matching. As expected, this feature efficiency reduces computer memory and processing time by orders of magnitude over the template-based approach. Therefore, the results of this thesis study reveal the DSC modeling approach to ATR to be superior to template matching in many ways and lay a ground work for further development of the DSC approach.

CHAPTER 6
Further Research

In my research, I have noted several topics which require further investigation. Some of these I have partially studied, and there are several I hope to investigate at a later time. These issues can be placed in three general categories of study: Electromagnetics, Signal Processing, and Pattern Recognition.

6.1 Electromagnetics

6.1.1 Cavity Responses

Currently, the DSC model does not include the ability to accurately model cavity responses such as those from engine intakes, cockpits, and open hatches. As I have stated, ATR may still be accomplished if the DSC model provides stable and discriminatory estimates of cavity returns for each target, but my confidence in this good fortune is naturally reserved. However, if cavity returns could be characterized in addition to the localized scatterers of the DSC model, the ability to discriminate between targets could be increased even further.

The difficulty with characterizing cavity returns is that there are resonant modes which "turn-on" at different frequencies. Consequently, it is possible for the magnitude of a cavity return to be non-linear, particularly over a large bandwidth. Thus, most scattering center models do not handle cavity returns explicitly and simply estimate cavities as a cluster of several scatterers.

6.1.2 Synthetic Radar Measurements

The ATR experiments in this thesis were performed strictly on measured data. Due to the expense and limited availability of radar measurements for some targets, however, many

ATR systems must train their classifiers on synthetic data created from an electromagnetic computer code such as XPATCH. Interestingly, some codes may actually model a target as a finite number of scattering centers similar to the ones that the DSC model estimates. In this case, it would be particularly valuable to analyze DSC modeling performance on these scattering-center based, synthetic measurements.

Since operational radar observations are always measured, there is an inherent flaw in training an ATR system with synthetic data. Both estimation and classification accuracies are dependent upon the fidelity of the data, and the impact of using synthetic data is certainly worth investigation.

6.1.3 Polarization

In general, a change in polarization will have a lesser effect on the DSC model characterization of a target than it does on the scattering center magnitudes in a range profile. However, a change in polarization can sometimes effect the type of scattering mechanisms which are measured on a target, particularly with regard to edge returns [13]. Therefore, polarization is definitely a consideration in DSC modeling. In addition, since more information can be gleaned from multiple polarization returns, these may be coordinated to improve DSC modeling of targets and improve ATR performance. Certainly the impact of polarization on ATR will always be studied and might be further scrutinized in the case of 1-D ATR by DSC modeling.

6.2 Signal Processing

6.2.1 Image Segmenting

If the image of a target could be segmented into a series of independent returns, then perhaps a more accurate and efficient DSC model estimation scheme might be implemented. At the extreme, one could apply the DSC model to the frequency response of one scattering center

peak at a time. This approach could simplify the choice of model order per peak to one or two scattering center estimates. I was encouraged by the advantage that this kind of peak-by-peak estimation would afford; however, I was not able to decouple the significant impact that truncating the time domain had on the representation of the target in the frequency domain, an inescapable consequence of image segmentation by peaks. Perhaps a viable approach to image segmentation could be discovered with further research.

6.2.2 Model Order

The DSC model order, as I have shown, has a large impact on target classification. Since one cannot perform classification by using a different number of features for each class, the model order must be the same for all targets of interest. I know that classification can be performed for underfit modeling of targets as demonstrated by this thesis. However, there may be a way to overfit, estimate too many scatterers, and then perform post processing to reject some scattering centers. For instance, one might reject scatterers with type parameter of $\alpha = -3$ or less. This should be possible; however, there is one major obstacle to this approach that would need to be addressed -- the processing time required to estimate increasingly higher-order DSC models quickly becomes unacceptable because all parameters are estimated simultaneously. Another obvious research area lies in developing an efficient way to estimate the model order a priori.

6.2.3 ATR Based DSC Estimation

The DSC modeling analysis performed by Chiang [9] focuses on modeling accuracy with only some considerations for speed. In an ATR application, this estimation algorithm could be adapted with the final classification process in mind. Thus, if classification accuracy, as opposed to parameter accuracy, is the goal, then perhaps a newer, faster algorithm could be developed for ATR applications. This research topic is constrained by the fact that reduced modeling accuracy will almost always reduce ATR performance.

6.3 Pattern Recognition

6.3.1 Low Observable Targets

In general the scattering mechanisms of low observable targets are of low magnitude and are typically dominated by corner diffractions. There is much further research that can be conducted to increase modeling accuracy of these mechanisms and separate them from noise and clutter. A statistics based analyzation of the DSC model would possibly allow such a development. Certainly this is an area of interest, for the radar absorbing materials used in low observable design can introduce new frequency dependencies other than those estimated by the DSC model.

6.3.2 Classifier Generalization and Flexibility

The ability of the DSC model to be used on problems with more than four classes is of interest. Also of interest is the ability to recognize both new targets and targets of same class but of different configuration (i.e. attached fuel tanks). For example, I could have trained my classifier on three of the four targets, leaving out the F-14f. Then to gauge how flexible my recognizer is, I could see if the F-14f would be correctly classified as an F-14, F-14b in this case. Studying the generalization and flexibility of a classifier is a worthy undertaking; however, to be done properly it requires data on more than four targets. Some data considerations are discussed in Appendix C.

APPENDIX A
Radar Imaging

One of my first tasks was to understand how my sponsor was using HRR images to perform ATR. Figure A.1 accurately depicts HRR and SAR image formation as basically Fourier transforms and magnitude calculations. Many ATR algorithms have had success in these two image domains, particularly SAR. To enable the reader to understand how radar images are formed, this appendix covers some basic radar imaging concepts related to this work. It begins by illustrating the relationship between phase history, HRR, and SAR data domains, and then describes each domain in depth.

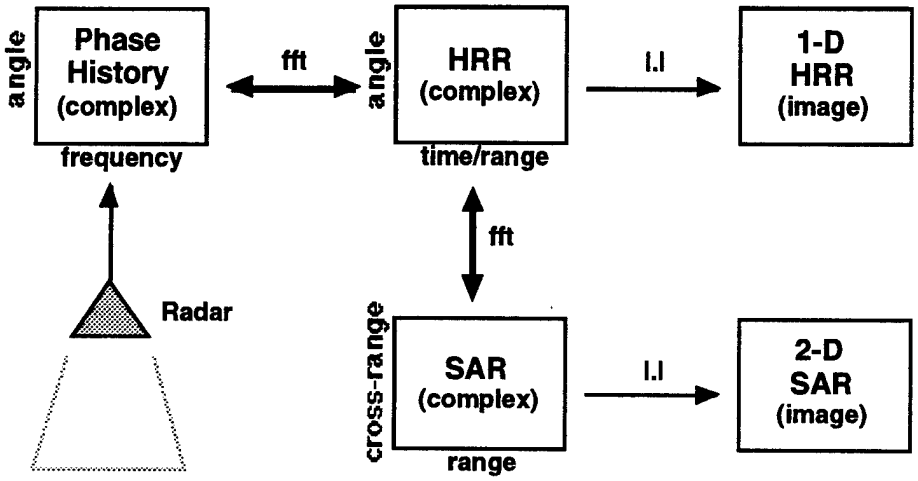

Figure A1: Radar imaging domain relationships

A.1 Phase History Domain

The Phase History Domain is a vector of the frequency responses of the entire scene, target and clutter, from different angles. Since the frequency responses are obtained from a "chirped" radar pulse, each frequency response is also a vector of complex radar returns at each

frequency in the "chirped" pulse. Therefore, this vector of vectors can be represented by an array of angle-frequency measurements as illustrated by the Phase History Box in Figure A.1. Since the measured E-field is complex-valued, note in Figure A.1 that the phase history is also complex.

Post processing can separate the frequency response of a target in the scene from clutter. A popular technique for clutter cancellation is Doppler processing. Doppler processing can differentiate moving targets from clutter if the targets have a different radial velocity from the radar than the clutter [12]. After the target has been isolated, the Phase History Domain is assumed to contain only the target's frequency response and additive noise.

A.2 HRR Domain

The HRR domain is created from the Phase History Domain by an inverse Fourier transform along each frequency response. A simple inverse discrete Fourier transform can be used if the frequency axis is linear. By this transformation, the frequency-axis becomes a time-axis. Furthermore, one can relate time to range by

$$x = 2\pi ft \tag{A.1}$$

where x is the down range distance from the zero phase reference in meters. Through this relationship, we obtain the range-axis and the complex HRR domain is created.

From the complex HRR matrix one can derive the impulse response or image of the target by examining the real part or magnitude of the HRR domain respectively. An absolute value sign, $|.|$, is given in Figure 12 to show how an HRR image is formed. An example HRR image of an F-4 military aircraft can be found in Figure 5.1a. The Fourier resolution of the range axis is given by

$$\Delta x = \frac{c}{2B} \tag{A.2}$$

where Δx is the Fourier resolution, c is the velocity of propagation, and B is the bandwidth of the frequency sweep [12]. Lastly, the maximum unambiguous range is given by

$$R = \frac{c}{2\Delta f} \tag{A.3}$$

This figure dictates the rate of frequency sampling necessary to prevent aliasing in the HRR image domain [12].

A.3 SAR Domain

The SAR domain is created from the HRR Domain by an inverse Fourier transform along the angle axis. This operation is not a simple transform, but requires a polar to Cartesian conversion in the Phase History Domain and "range walk" compensation to provide a focused image [14]. Through this final Fourier transform, the angle-axis becomes a cross range-axis as shown in the complex SAR matrix of Figure A.1. From this matrix one can again derive the impulse response or image of the target. An absolute value sign, $|.|$, is given in Figure A.1 to show how a SAR image is formed from the complex SAR domain. Since the transformations used to obtain the complex SAR domain are almost always linear, it is possible to invert these transformations to obtain both the HRR and the Phase History domains from the complex SAR domain.

APPENDIX B
Pattern Recognition

Pattern Recognition evolves from the study of statistically based decision methods. These decision methods can produce machine-intelligence as advanced as automated vision. The goal of pattern recognition is to classify objects of interest called patterns into one of a number of categories called classes. Generally, this classification is automated on a computer [15].

B.1 Feature Extraction

In order to distinguish between classes, we identify features which both accurately describe and differentiate between classes. We assume that we have some prior knowledge of how to discriminate between classes. This prior knowledge will govern completely how one chooses their features. If each feature is a dimension in space, one can define regions which contain all of the observations of one class as shown in Figure B.1.

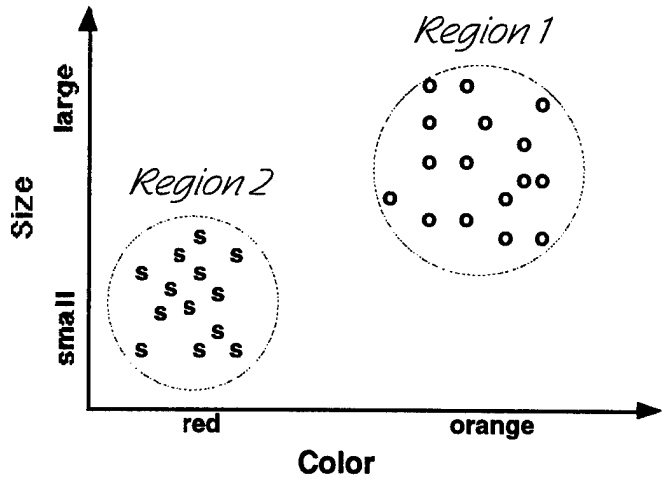

Figure B.1. Example feature space (Region 1 is oranges; Region 2 is strawberries).

In the case of vision systems such as those in ATR, geometrical features tend to separate objects very well.

Feature extraction is applied to all of the data in an attempt to capture the discriminatory information between classes by eliminating non-discriminatory, noisy information. This extraction is problem specific and includes computational considerations.

B.2 Training

After a feature set has been identified, it is time to train the pattern recognizer. A diagram of the supervised learning process is given in Figure B.2.

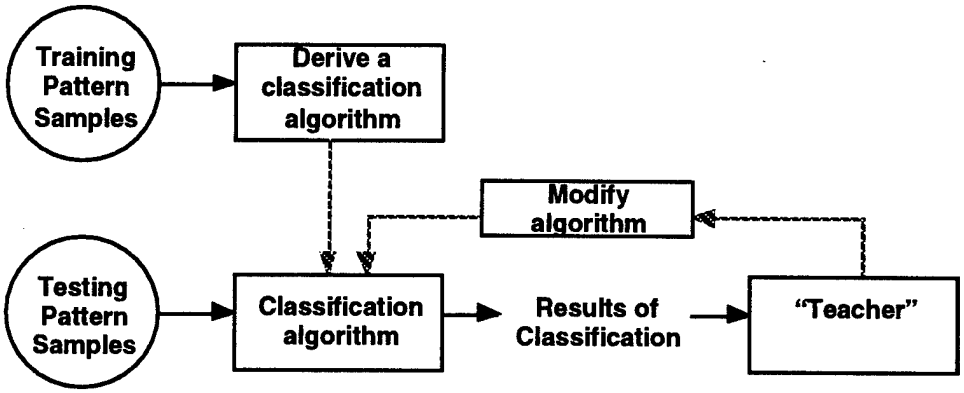

Figure B.2. Diagram of the supervised learning process [15]

Supervised learning requires that the Pattern Samples are labeled by class, while unsupervised learning, or clustering, does not require labeled data. To train our classifier, a statistically significant, large number of observations for each class are required. This large number of observations will adequately characterize the regions as portrayed in Figure B.1. In the extreme case, it is obvious that a single sample "o" does not effectively represent the population of Region 1, although several samples begin to accurately represent the region.

When training the classifier, the machine architecture, distance function, and learning algorithm are key factors. Architecture for parametric pattern recognition can include anything from the baseline Gaussian classifier to neural nets of various types. The classic distance

functions are Euclidean, Maholanobis, and absolute value [15]. Learning algorithms use all of the training data to set the parameters of the recognizer and often this will be an iterative procedure. Again, these engineering decisions are problem-specific.

B.3 Testing

Testing involves recording the performance of the fully-trained algorithm on a subset of data which was not used for training the classifier. The same feature extraction, is of course, performed on the test measurements. One always uses labeled test data even though classes which were not used to train the classifier may be used in testing. Testing the classifier involves simply classifying the test data using the same distance metric, but not updating the classifier's parameters – no learning is going on here. Since the data are labeled, one can track the performance of the classifier on all test samples. From these results one forms a confusion matrix which summarizes the classifier's performance for recognizing each class. An example confusion matrix is given in Figure B.3.

		classified as:			
		w1	w2	w3	w4
true class:	w1	90.3 %	1.7 %	3.5 %	4.5 %
	w2	6.9 %	86.1 %	1.4 %	5.6 %
	w3	0.8%	1.3 %	97.2 %	0.7 %
	w4	0.3 %	1.5 %	2.6 %	95.6 %

Figure B.3: Example confusion matrix

Notice that there are 100 % of the samples of each true class represented in the matrix, a percentage reached by adding up the horizontal lines. Performance of the classifier is most easily gauged by examining the matrix diagonal of correct classification percentages – the higher these values are, the better the recognizer. With these basic pattern recognition concepts in

mind, one now have an ability to discuss approaches to solve the 1-D ATR problem, including template matching and the DSC model approach presented in this thesis.

APPENDIX C
MSTAR Data Study

This appendix is included to record my efforts to perform ATR on the MSTAR data set. However, it also serves as a case study in using the DSC model on typical radar image data. The publicly-released MSTAR data set consists of a series of SAR images over a full 360 degree azimuth cut at two different elevations, 15 and 17 degrees. The images are of several stationary military ground vehicles and the complex SAR domain is available. As I stated in Appendix A, if the complex SAR domain is available, it can be used to construct the original phase history measurements by reversing all of the linear processing steps and transformations which were applied to the data to obtain the SAR domain. However, the original phase history measurements for any radar data set, if available, should always be used before attempting to reverse the often complex post processing implemented to create SAR images.

In the case of the MSTAR data set, the original phase history measurements were not contractually required to be delivered to Sandia National Laboratories, and its availability to the government is limited. In fact, its existence is in question due to the on-platform image processing that the contractor implemented when the data was collected. Because the DSC model is a frequency domain model, exact phase history must be available. Furthermore, measurement error or corruption will devastate the DSC model's ability to provide an accurate representation of the target. As stated in Section 4.3, poor DSC modeling is a strong indicator of measurement error.

C.1 Phase History Complications

My attempts to reverse signal process the MSTAR data were largely based on the work which Wright Laboratories has already done in this area. Although Wright Laboratories has addressed many of the issues in recreating the MSTAR phase history, they have not addressed

all of them because phase history data is not important to performing template matching ATR. This section summarizes the major complications which I encountered while using the MSTAR data for ATR based on the DSC model.

C.1.1 Frequency Sampling

I have not been able to determine what the original frequency sampling of the MSTAR data was. I know the center frequency is 9.6 GHz, the bandwidth is 591 MHz, and the frequency sweep is linear (all of these are listed in the header of the MSTAR data on CD-ROM), but I do not know the frequency step, Δf, between samples. I have been told by Wright Labs that the original measurement can be represented by the center 101 elements (unpadded) in the phase history, but I am not sure if element-for-element these correspond to the original samples in frequency that were measured. If there exists an element-for-element correspondence, then Δf is about 50 MHz; if not, then any interpolation may corrupt the frequency domain, destroying the DSC model's ability to analyze the target.

C.1.2 Zero Padding

The effect of zero padding allows the image to appear smoother and better sampled. Furthermore, zero padding is often used because most computers implement a circular discrete Fourier transform (DFT) when performing an FFT. Any padding may be removed from the data if the nature of the padding is known. If the data is padded with noise, or other special padding is used, the type of padding must be considered in order for proper inversion back to the phase history measurements. Unfortunately, the type and amount of padding that was used in the MSTAR data set is not explicitly known. Based on correspondence with Sandia National Laboratories (SNL), the best guess is that the phase history was zero padded with a cross to generate 128 rows and 128 columns.

C.1.3 Taylor Weighting

To form the SAR image, the MSTAR phase history is -35 dB Taylor weighted in both dimensions, angle and frequency, before applying the two dimensional Fourier Transform. This step is done in SAR processing traditionally to reduce sidelobes in the image. Keeping this in mind, I basically have two unanswered questions about how the weighting was applied:

1. Was it applied to the rectilinear or polar representation of the phase history?
2. Was it applied to the zero padded (128 elements) Phase History or the original (assumed 101 elements), unpadded data?

I would assume that the weighting was applied to the rectilinear, unpadded phase history as does Wright Laboratories in their work. However, I encountered some interesting results when I applied the inverse weighting to the zero padded (128 x 128 element) phase history. My attempt to apply inverse weighting to the zero padded data was spurred by the poor results I achieved using the non-padded inverse (101 x 101 elements) that Wright Laboratories was using. I noticed that the non-padded inverse weighting was creating graded peaks in the corners of the phase history data (101 by 101 elements) which appeared to occur from too much deweighting in the data. However, the graded peaks disappeared when I applied the inverse weighting to the padded (128 x 128) phase history. Essentially, this larger-area inverse weighting allowed the aforementioned corner peaks to be thrown away when unpadding the data down to a 101 x 101 phase history domain.

C.1.4 Focusing

There are several image processing steps which can help focus a spotlight SAR image. Spotlight SAR defocusing is primarily caused by taking a Fourier transform of each row and column of phase history data without first transforming the polar data rectilinear coordinates. Although the type of focusing used on the MSTAR data has been published, I have not yet tried to invert this transformation.

C.1.5 Speckle Reduction

There are several ways to reduce speckle in a SAR image. One of the more easy and popular ways to implement speckle reduction involves replacing the original phase measurement in frequency with a random phase across all samples. Since the SAR image is formed by taking the magnitude of the complex SAR domain data, this randomization in phase reduces speckle in the image. Such speckle reduction can provide significant improvement in radar imaging, seemingly adding contrast to the image, and allowing objects to be more easily seen. Therefore, speckle reduction is a particularly important goal in mapping radars where many objects are included in the field of view. Unfortunately, if this type of speckle reduction was implemented on the MSTAR data, it is not reversible.

C.1.6 Filtering

In an attempt to obtain a high-quality SAR image, many filters can be applied to the phase history measurements. Although I have heard rumors of various imaging filters being used on the MSTAR data, I have not seen this issue satisfactorily addressed. If a filter is known to have been implemented, then it is likely that its effects can be reversed, enabling the original frequency measurements to be obtained.

C.2 Clutter Cancellation

The need for clutter cancellation is not limited to 1-D ATR. By their nature, clutter returns are unpredictable and difficult to characterize, thereby providing no discriminatory information between targets. Consequently, 1-D ATR algorithms typically assume "target only" radar measurements with little to no clutter. These clutter canceled measurements can easily be obtained via Doppler processing for moving targets. Therefore, 1-D ATR is usually proposed for recognizing moving targets based on the assumption that non-moving targets are of less concern operationally.

In contrast, SAR images, such as the MSTAR data, always include clutter and additionally prefer stationary targets. Since the MSTAR data is SAR imagery including clutter, it is not ideal for 1-D ATR. Furthermore, since clutter can potentially be cropped from a range profile, MSTAR data may be used to perform template matching ATR. However, clutter returns cannot be cropped from the frequency domain and will impact a DSC approach to ATR.

The existence of clutter does not entirely preclude the use of the DSC model for ATR experiments using the MSTAR data set. Low energy clutter returns, such as those found in the MSTAR data, will potentially be ignored in an underfit DSC model (although there will be some indirect impact on accurate type estimation), while an overfit model will include scattering centers contained in the clutter (outside of the target extent) in its estimation. These spurious clutter scatterers will become noisy features which do not discriminate well between targets, and they will severely degrade ATR performance. Clutter cancellation and the phase history complications that I listed in this chapter must be addressed before the DSC model or any superresolution technique can be used to perform ATR on the MSTAR data set.

BIBLIOGRAPHY

[1] H.-J. Li and S.-H. Yang, "Using range profiles as vectors to identify aerospace objects," *IEEE Trans. Antennas Propagat.*, vol. 41, pp. 261-268, Mar. 1993.

[2] P. B. Silverstien, O. S. Sands and F. D. Garber, "Radar target classification and interpretation by means of structural descriptions of backscatter signals," *IEEE AES Systems Magazine*, pp. 3-7, May 1991.

[3] M. P. Hurst and R. Mittra, "Scattering center analysis via Prony's method," *IEEE Trans. Antennas Propagat.*, vol. 35, pp. 986-988, Aug. 1987.

[4] R. Carriére and R. L. Moses, "High resolution radar target modeling using a modified Prony estimator" *IEEE Trans. Antennas Propagat.*, vol. 40, pp. 13-18, Jan. 1993.

[5] J. J. Sacchini, W. M. Steedly and R. L. Moses, "Two-dimensional Prony modeling and parameter estimation," *IEEE Trans. Signal Processing*, vol. 41, pp. 3127-3137, Nov. 1993.

[6] Y. Hua and T. K. Sakar, "Matrix Pencil method for estimating parameters of exponentially damped/undamped sinusoids in noise," *IEEE Trans. Acoustic, Speech, Signal Process.*, vol. 38, pp. 814-824, May 1990.

[7] A. Moghaddar, Y. Ogawa, and E. K. Walton, "Estimating the time-delay and frequency decay parameter of scattering components using a modified MUSIC algorithm," *IEEE Trans. Antennas Propagat.*, vol. 42, pp. 1412-1418, Oct. 1994.

[8] L. C. Potter, D.-M. Chiang, R. Carriére, and M. J. Gerry, "A GTD-based parametric model for radar scattering," *IEEE Trans. Antennas Propagat.*, vol. 43, pp. 1058-1067, Oct. 1995.

[9] D.-M. Chiang, "Parametric signal processing techniques for model mismatch and mixed parameter estimation," Ph.D. dissertation, The Ohio State Univ., Columbus, 1996.

[10] J. B. Keller, "Geometric theory of diffraction," *J. Opt. Soc. Amer.*, pp. 116-130, Jan. 1962.

[11] R. Prony, "Essai experimental et analytique sur les lois de la dilatabilite de fluides elastiques et sur celles de la force expansion de la vapeur de l'alkool, a differents temperatures, "*J. L'Ecole Polytech*, vol. 1, pp. 24-76, 1795.

[12] D. R. Wehner, *High Resolution Radar*. Boston: Artech House Inc., 1987.

[13] E. F. Knott, J. F. Shaeffer, and M. T. Tuley, *Radar Cross Section*. Boston: Artech House Inc., 1993.

[14] W. G. Carrara, R. S. Goodman, and R. M. Majewski, *Spotlight Synthetic Aperture Radar*. Boston: Artech House Inc., 1995.

[15] C. W. Therrien, *Decision Estimation and Classification*. New York: Wiley, 1989.

REPORT DOCUMENTATION PAGE

Form Approved
OMB No. 0704-0188

1. AGENCY USE ONLY *(Leave blank)*	2. REPORT DATE	3. REPORT TYPE AND DATES COVERED
	December 1997	Master's Thesis

4. TITLE AND SUBTITLE
A DISPERSIVE SCATTERING CENTER, PARAMETRIC MODEL FOR 1-D ATR

5. FUNDING NUMBERS

6. AUTHOR(S)
Dane F. Fuller, First Lieutenant, USAF

7. PERFORMING ORGANIZATION NAME(S) AND ADDRESS(ES)
Air Force Institute of Technology
2750 P Street
WPAFB, OH 45433-7765

8. PERFORMING ORGANIZATION REPORT NUMBER
AFIT/GE/ENG/97D-05

9. SPONSORING/MONITORING AGENCY NAME(S) AND ADDRESS(ES)
WL/AACR
2010 5th Street, Bldg 23
WPAFB, OH 45433

10. SPONSORING/MONITORING AGENCY REPORT NUMBER

11. SUPPLEMENTARY NOTES

12a. DISTRIBUTION AVAILABILITY STATEMENT
Approved for public release; distribution unlimited

12b. DISTRIBUTION CODE

13. ABSTRACT *(Maximum 200 words)*

The dispersive scattering center (DSC) model characterizes high-frequency backscatter from radar targets as a finite sum of localized scattering geometries distributed in range, these geometries, along with their relative locations, can be conveniently used as features in a one-dimensional automatic target recognition (ATR) algorithm. The DSC model's type and range parameters correspond to geometry and distance features according to the geometric theory of diffraction (GTD). Since these parameters are estimated in the phase history domain of the radar signal, the range parameter does provide superresolution in the time domain.

To demonstrate the viability of feature extraction based on the DSC model's range and type parameters, a four class ATR experiment was performed. The experimental data contains 301 direct range measurments each for four model aircraft of similar size and shape at 0 degrees elevation and from 0 to 30 degrees azimuth. After implementing DSC model feature extraction on this data, a fully-connected, two-layer nueral net obtained over 98% classification accuracy. In addition, DSC model feature extraction offers an approximate 85% reduction in the number of features compared to the numerous Fourier bin magnitudes in template matching approaches to ATR.

14. SUBJECT TERMS
Automatic Target Recognition (ATR), Superresolution, Neural Net, High Resolution Radar (HRR), Radar Scattering, Range Profile

15. NUMBER OF PAGES
66

16. PRICE CODE

17. SECURITY CLASSIFICATION OF REPORT	18. SECURITY CLASSIFICATION OF THIS PAGE	19. SECURITY CLASSIFICATION OF ABSTRACT	20. LIMITATION OF ABSTRACT
UNCLASSIFIED	UNCLASSIFIED	UNCLASSIFIED	UL